Acoustic emissions from in situ compression and indentation experiments on sea ice

Ben Lishman[1], Aleksey Marchenko[2], Peter Sammonds[3], Andrii Murdza[4]

(1) School of Engineering, London South Bank University, Borough Road, London, SE10AA, UK; ben.lishman@lsbu.ac.uk
(2) Department of Arctic Technology, University Center in Svalbard, Longyearbyen, Norway
(3) Institute for Risk and Disaster Reduction, University College London, Gower Street, London, WC1E 6BT, UK
(4) Ice Research Laboratory, Thayer School of Engineering, Dartmouth College, Hanover, NH, USA

Abstract

We present results from measurement of acoustic emissions (AE) during compression and indentation of natural sea ice in situ. We show that AE amplitudes are associated with load, so that periods of loading and unloading, and cyclic oscillations in loading during indentation, can be determined from AE records as well as from load measurements. We show that AE measured during these experiments obeys Gutenberg-Richter-type scaling laws, implying that the crack distribution within the sea ice is self-similar. We show that b-values, which indicate the ratio of small cracks to large cracks, decrease during loading, tending towards a value around 1 at failure, and increase again when loading is removed. This suggests that AE can be used to measure, non-invasively, damage and healing of natural sea ice. We conclude by discussion practical applications of these results, and opportunities for further development of AE measurement as a tool for understanding cracking in ice.

Keywords

Acoustic emissions; fracture; sea ice.

Introduction

When sea ice is deformed at high strain rates, it fractures. This fracture occurs when individual small cracks grow numerous and form a continuous network. Each of these small cracks, as it forms and grows, releases energy as a pressure (or stress) pulse within the ice. These pulses, or 'acoustic emissions' (AE), therefore, can provide information about the development of cracks within the ice, and may be helpful in understanding and predicting ice breakup.

The basis of AE measurement is intuitive: materials make sounds when they break, and these sounds may provide information about the way the material deforms. Seismology, and the history of seismograms, can be considered as a precursor to acoustic emissions monitoring. The first scientific investigations of AE were made by Kishinoue, 1934 (published in English 1990), and later by Kaiser in 1950, who examined a range of metals and found that AE frequency and amplitude were, for a given material, related to stress levels (Liptai et al., 1970). Since then, acoustic emissions have been widely used to understand the behaviour of materials, and entire journals are dedicated to the field today. Alongside their applications in materials research, AE measurements are used in structural health monitoring of machinery and infrastructure. One important feature of this monitoring is that it can be conducted non-invasively, since sensors can be attached to the surface of structures.

Acoustic emissions caused by failure of Arctic sea ice have been recorded in the Arctic ocean and are well-analysed (e.g. Langley, 1989; Xie and Farmer, 1991). However, these studies have typically measured at low frequencies (<20kHz) in order to capture the effects of large-scale ice breakup. Analysis of smaller-scale behaviour requires analysis at higher frequency (Langhorne and Haskell, 1996). Experiments at these frequencies have been conducted during compression tests on polycrystalline ice (St Lawrence and Cole, 1982) and on multiyear sea ice (Sinha, 1985); during constant load creep experiments on sea ice (Sinha et al., 1992); to observe loading due to vehicle movement on ice (Langhorne et al., 1990); during fracture of cantilever beams (Langhorne et al., 1993); and during creep measurements on first year sea ice (Sinha, 1996). Langhorne et al., 1996, show that AE due to microcracking in a deformed beam of first year sea ice is correlated with the applied load. They show that the AE measurements follow a magnitude-frequency relationship comparable to well-known seismological models. The authors also note that sound attenuation increases with frequency, and so for high frequency measurements, sensors must be located close to the source.

Cole and Dempsey, 2004, report measurements of acoustic emissions around the tip of a developing crack, propagated in mode I by cyclic loading. They find significant acoustic activity in the crack tip area before they observe macroscopic propagation of the crack tip. In this work the propagation distance over which AE could be detected was shown to be less than 0.25m (at acoustic frequencies which can be estimated from figure 8 around 1MHz). Cole and Dempsey (2006), analysing field cores under cyclic loading, note that "sea ice experiences an extensive amount of microcracking at stress levels that are well below its tensile failure stress level." They also hypothesise that microcracking occurs initially in a distributed manner, before eventually becoming concentrated in low strength regions after continued deformation. Cole and Dempsey observe a "substantially greater" number of acoustic events in tension vs compression.

Acoustic emissions have been used more widely in ice laboratories, where it is easier to eliminate noise and to manage sensitive equipment (e.g. Gold, 1960; Sinha, 1982; Rist and Murrell, 1990; Weiss and Grasso, 1997; Li and Du, 2016). From these experiments we know that AE techniques can be used to distinguish between failure methods in ice. For example, Li and Du (2016) show evidence that tensile and shear cracking can be distinguished based on the properties of the emitted acoustic signals.

In this work we show results from a large new AE dataset (encompassing tens of thousands of acoustic hits) recorded from natural sea ice, deformed *in situ* by mechanical actuation, in the Van Mijen Fjord, Spitsbergen. In the first experiment presented, ice is compressed by a flat indentation plate, and in the second experiment, ice is crushed by a semicylindrical indenter.

Overview of experiments

The experiments documented in this paper were conducted on the Vallunden lake, connected to the Van Mijen Fjord, Svalbard, on the 8th of March 2016. The sea water salinity in the lake was 34-35ppt, and the ice salinity was measured as 4.4ppt. The ice formed as natural sea ice, with a granular top surface and a columnar structure beneath, with grain sizes of a few millimetres. Thin sections from ice cores taken nearby in the fjord can be seen in Karulina et al., 2019. The ice thickness during the experiments was 600mm. The ice temperature, measured with a thermistor string frozen close to the experiments, and averaged across the thickness of the ice, was -2.4°C, and the air temperature was around -10°C (Marchenko et al., 2018).

The ice sheet was cut with hand saws to leave desired configurations of ice and open water, so that the ice can be loaded in-plane and deformed. Given the thickness of the ice sheet, we do not believe that the ice used in our experiments was significantly damaged during this phase of saw-cutting and preparation. This loading was carried out with a bespoke rig, consisting of two Enerpac 30T hydraulic cylinders, controlled by field laptop and powered from a three phase generator. The applied load was measured with load cells installed inside the hydraulic cylinders and recorded onto the field laptop. The displacement of the actuators was measured on internal displacement sensors and recorded along with load data.

Acoustic emissions were recorded using a Vallen AMSY5 system. We used PZT-5H compressional crystal sensors (Boston Piezo-Optics inc., 15mm diameter, 5mm thickness, 500kHz centre frequency), potted in epoxy. These AE sensors were then placed into shallow drilled holes (~20mm deep) in the ice surface, and allowed to freeze. The piezo crystals convert acoustic signals into electrical signals, which were amplified locally (on Vallen preamps with a 40dB gain) and then transmitted to the AMSY5 central processing unit. When the signal on any channel exceeded a certain threshold, a “hit” was recorded: the AMSY5 unit records the sound wave for 400μs, at a sampling rate of 5MSs^{-1}. For each hit, certain characteristics are determined by Vallen software: the time of arrival (at the piezo sensor), amplitude, duration and rise time. In post-processing, the frequency content of the recorded transient can be calculated by FFT for each hit, and from this the peak frequency of the transient can be determined. Based on spot checks, signals with peak frequencies greater than 180kHz were considered to be noise, and were filtered out of the results

shown here. The system has a low frequency cutoff at 100kHz, so all signals shown here represent emissions with a central frequency in the range 100-180kHz. Acoustic measurements and load measurements were recorded on separate systems, without a calibration signal, and so the time calibration between them is only accurate to ±1s.

In separate experiments using a pulser and receiver, the sound wave speed in the ice was calculated to be 3300ms^{-1}. The frequency range we are measuring in (100-180kHz) therefore corresponds to wavelengths from 18mm to 33mm. Sound attenuation in the ice was not measured and is not accounted for in this paper (this is discussed further below). Background acoustic noise levels can be seen at the start of each set of experimental data: these were non-zero but small compared to acoustic signal levels during loading.

Appendix A shows results from a simple tensile test, to allow a single acoustic hit, along with its transient and FFT, to be seen and understood in context.

Compression testing

Setup

In this experiment a flat steel plate compresses a cutout section of the level ice in-plane, as shown in figure 1. The steel plate is 600m wide, 800mm high, and positioned so that it extends across the vertical extent of the sea ice. Slush and floating ice are cleared, and the plate is placed in direct contact with the saw-cut edge of the ice. The load is applied at a constant deformation rate of 1mm/s. The strain rate and peak compressive stress are calculated as approximately $1\times10^{-3}s^{-1}$ and 1MPa respectively (Marchenko et al., 2018). Detailed loading patterns are shown later in this paper, and discussed further in Marchenko et al., 2018. Acoustic emissions are recorded on four channels: channel 1 is the closest to the plate, channel 2 is furthest from the plate, and channels 3 and 4 are off-centre on the ice, as indicated. The transducer for channel 1 is 240mm from the plate, and the transducer for channel 2 is 1050mm from the plate, as shown in figure 1c.

(a) photo

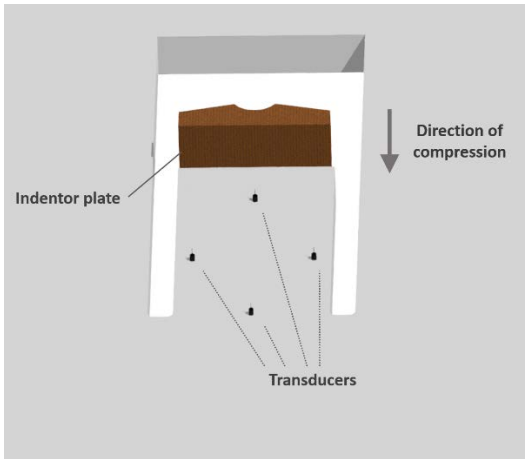

(b) photo annotation

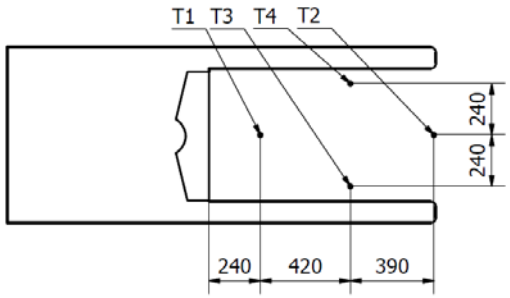

(c) dimensioned plan view

Figure 1: the in situ compression experiment.

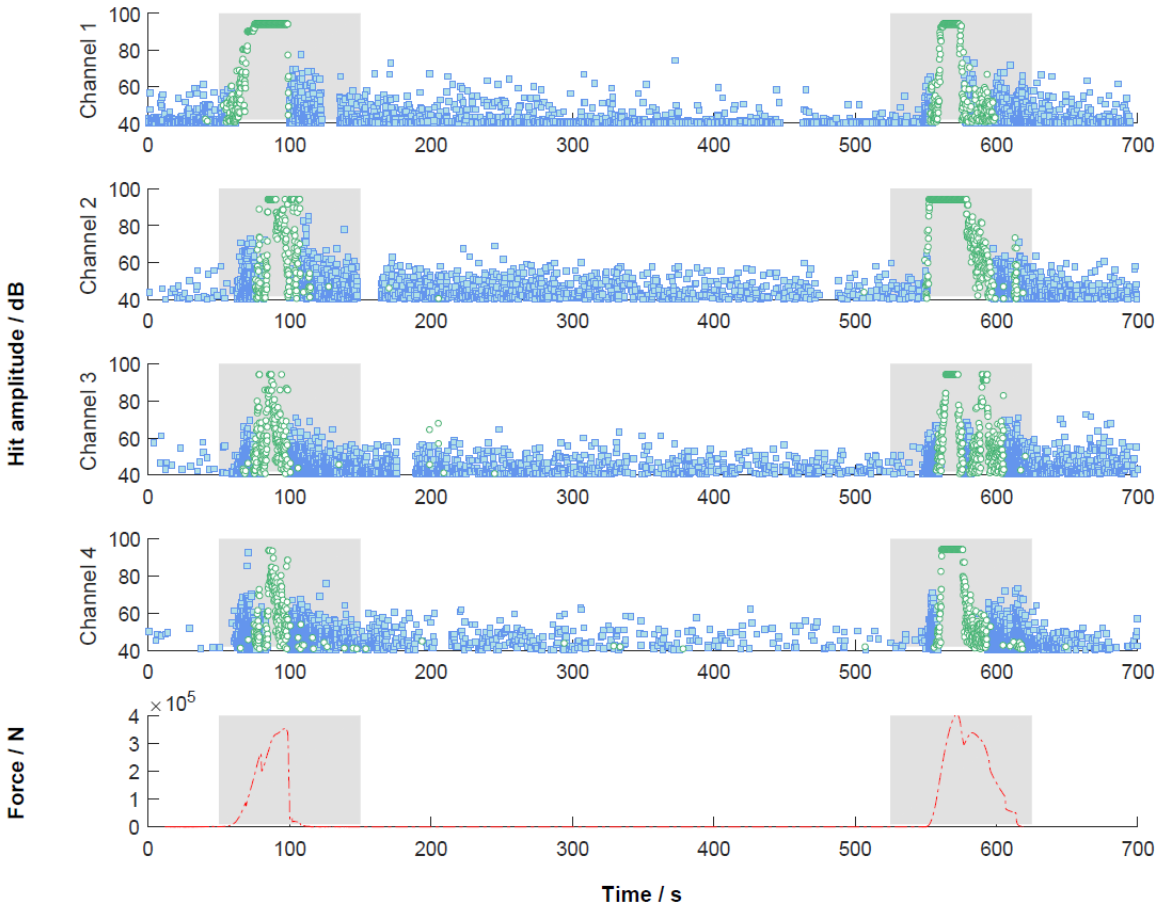

Figure 2: acoustic emissions (top four plots, showing amplitude of hits on channels 1-4) and force (bottom plot) against time for the compression experiment described above. Loading occurred in two separate phases, shaded in this plot. The shaded regions are shown in more detail in figure 3 (50-150s) and figure 4 (525-625s). Round green unfilled markers indicate hits where no transient was recorded: typically these are associated with periods of intense AE, and we attribute them to saturation in the electronics. The shaded regions are shown in more detail in figure 3 (50-150s) and figure 4 (525-625s).

Results

Figure 2 shows results from the compression experiment: the top four plots show acoustic emission amplitude (measured on the Vallen for each of the four transducers) as a function of time, and the bottom plot shows the applied force (measured on load cells in the hydraulic actuators) as a function of time. On the AE plots, square blue markers show hits which were fully recorded, while round green markers show hits where only the amplitude was recorded. The second category of recording, where only an amplitude is recorded (and no transient), tend to occur during periods of high loading and high levels of AE, and are associated with saturation in our equipment. In later analysis and further data processing, only the fully recorded data are used.

Loading was applied over two separate intervals, separated by nearly ten minutes (during this gap the loading actuator positions were adjusted to ensure symmetric loading). The first loading interval occurred from around 50-100s, and the second, from around 550-620s. The AE and load records during these periods are shown in more detail in figures 3 and 4.

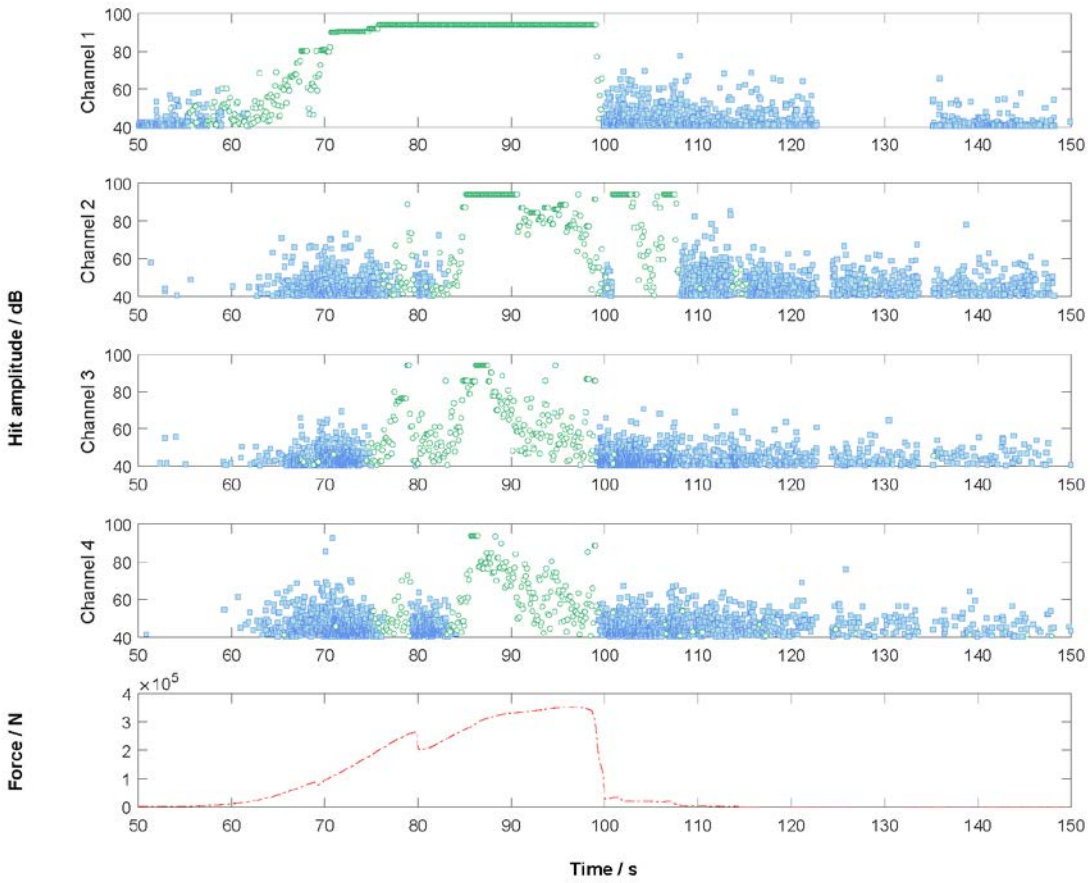

Figure 3: acoustic emissions and force against time for the compression experiment shown above, focussing on the first period of loading, from 50-150s.

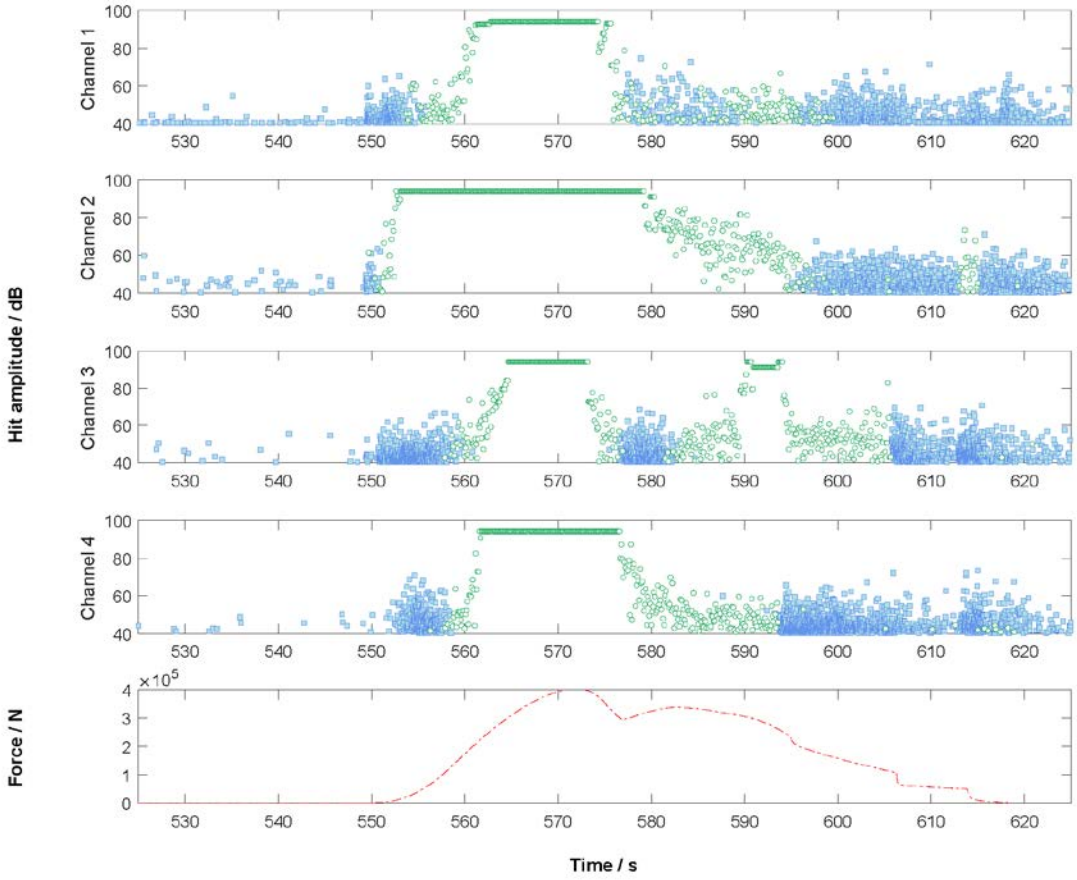

Figure 4: acoustic emissions and force against time for the compression experiment shown above, focussing on the second period of loading, from 525-625s.

Indentation testing

Setup

Figure 5 shows the experimental setup for our indentation experiment. A semicylindrical indenter is fixed onto the hydraulic actuators. The indenter is 150mm in diameter and 800mm in height, positioned so that it extends across the vertical extent of the sea ice. The indentation is applied at constant speed of 0.45mm/s. The geometry of the experiment means that the force is applied over a much smaller area than in the compression test above, and so stresses in the ice are higher. The strain rate and peak compressive stress are calculated as approximately $1.5\times10^{-3}s^{-1}$ and 5MPa respectively (Marchenko et al., 2018). In this experiment the indenter moved through the ice as it crushed it, and the total displacement of the indenter head was around 200mm. Detailed loading patterns are shown later in this paper, and discussed further in Marchenko et al., 2018. The acoustic transducers in this experiment are located 1m from the zone of indentation, as shown in figure 5c.

(a) photo

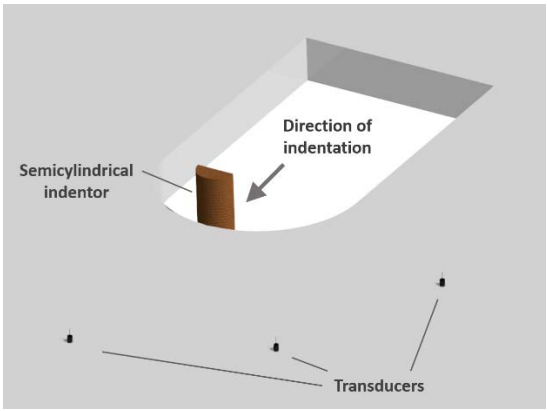

(b) photo annotation

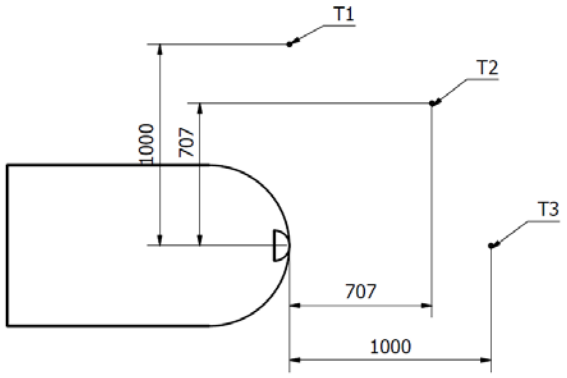

(c) dimensioned plan view

Figure 5: the in situ indentation experiment. (Note that in the photo, the rightmost AE transducer is hidden behind a leg of the actuator support frame.)

Results

In this experiment, AE is recorded on three channels. AE hit amplitudes as a function of time (top three graphs, showing three channels), and load as a function of time (bottom graph), are shown in figure 6. Cyclic patterns in the load were observed after around 300s: these are a response to loading (rather than a deliberately applied variation in the loading).

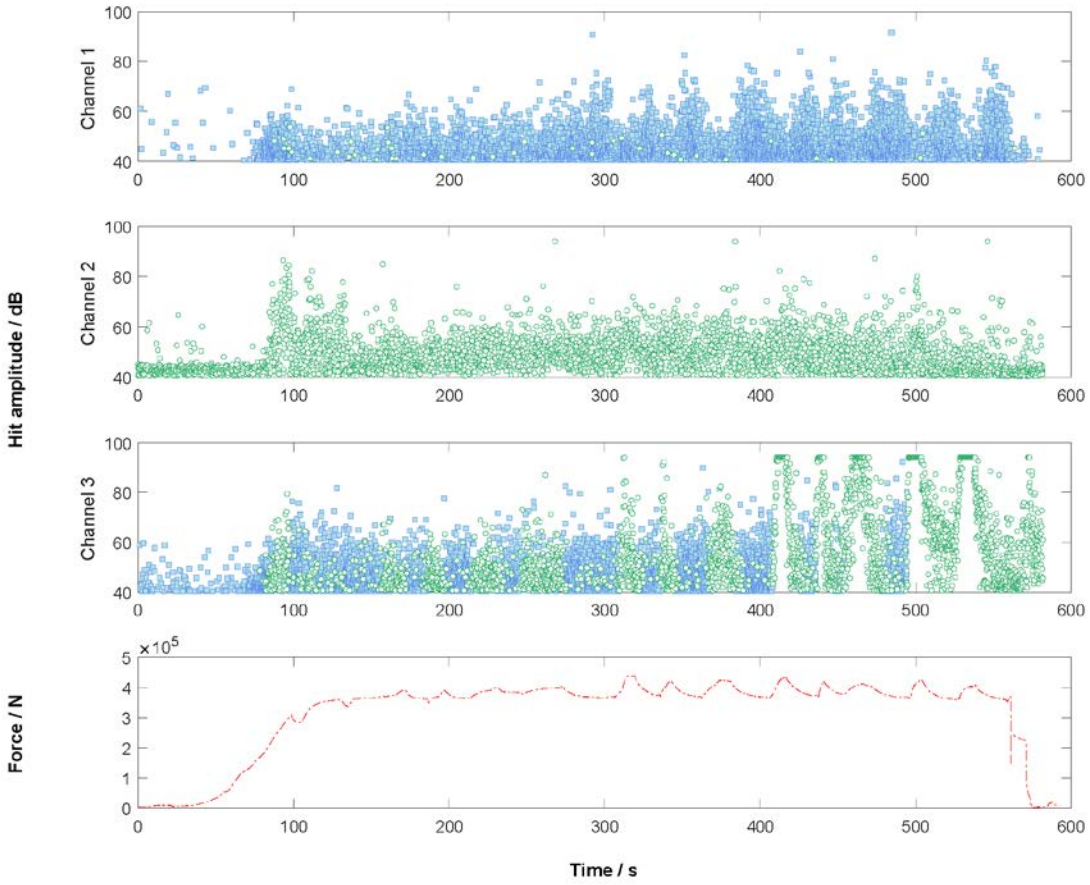

Figure 6: hit amplitude as a function of time, across three channels. Cyclic behaviour which can be seen in the force measurement is also observed in the acoustic emissions on channels 1 and 3. It seems that the acoustic emissions on channels 1 and 3 may be out of phase with each other during this cyclic loading. Round green unfilled markers indicate hits where no transient was recorded: typically these are associated with periods of intense AE, and we attribute them to saturation in the electronics. No transients were recorded on channel 2 due to an instrumentation problem, and so we focus on channels 1 and 3 in further analysis.

Analysis

Hit amplitudes against time

Hit amplitudes and hit quantities appear to vary with loading. In both tests shown, periods of higher force also show increased hit amplitudes and greater numbers of hits. This relationship between loading and AE is also seen clearly in the simple example shown in appendix A. In figure 3, we see very few hits before 60s, although there are some, probably corresponding to background noise, thermal deformations, wind, waves, human actions etc. Beginning around 60s, as the load begins to rise, the maximum amplitudes of acoustic emissions also begin to rise until saturation occurs. We then see continued saturation until the load drops off at around 100s. After the load is removed, AE signals remain elevated and decay over >100s. A similar fall-off in AE rate after loading is described by a power law in Sammonds et al., 1994. Mansurov (1994) attributes post-failure AE in rocks to “stress redistribution”. It is also possible that the post-failure AE in our experiments are

caused by collisions and sliding between loose pieces of ice. However, this is difficult to reconcile with the elevated AE from 100-150s in the compression experiment, where the ice was not visibly damaged.

The same relationship between AE and load – few AE hits before loading, increasing AE with increasing loading, a peak of AE around the maximum load, and elevated AE after loading is removed - is seen in figure 4. In figure 6, we see again a similar relationship between loading and AE hit amplitude and hit counts. Notably, in figure 6, where there is a period of cyclic oscillations in the load after around 300s, we see corresponding cyclic variations in the AE record, particularly on channels 1 and 3. The cyclic oscillations in the load may be related to ice spalling, and similar phenomena may be responsible for ice-induced vibrations (Gagnon, 2012), and so it is useful to note that AE measurements allow us to record these phenomena non-intrusively. Overall, it seems reasonable to state that AE measurements allow us to infer when loading started and finished, and when peaks in the load occurred.

b-values, and ratios of low amplitude events to high amplitude events

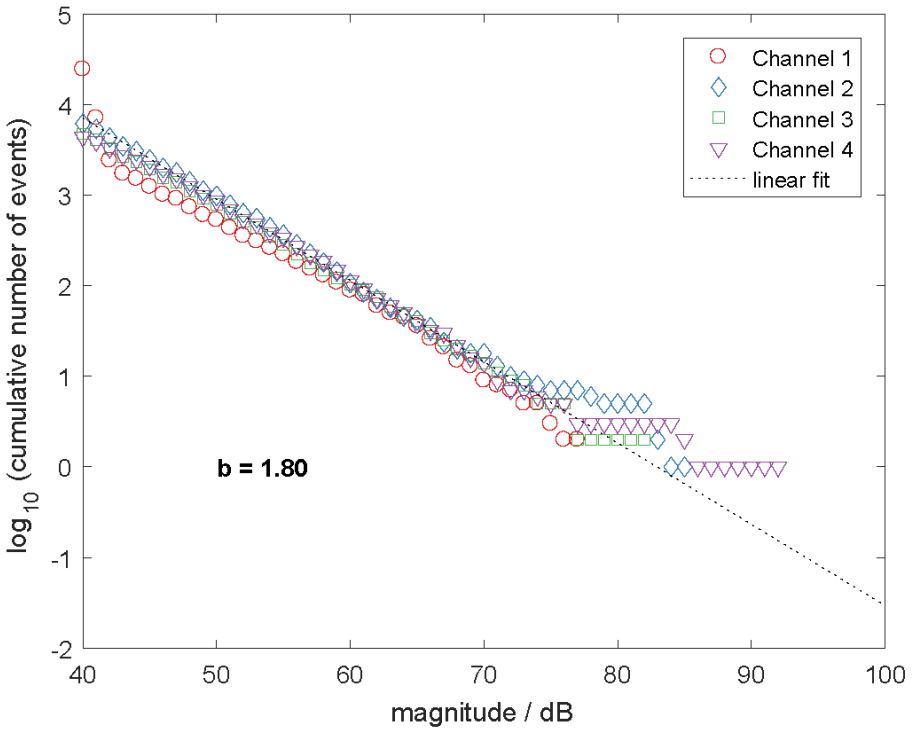

Figure 7: cumulative magnitude distribution for the AE hits from the compression experiment shown above (the data cover the entire duration of the experiment). The best-fit straight line is matched to the data from channel 2, up to 70dB magnitude, and has a slope $b = 1.80$.

Within any window of AE measurements, we expect to find a small number of relatively high amplitude hits, and a greater number of low amplitude hits. The understanding of these patterns of AE amplitude originated in seismology, where the behaviour is modelled by the Gutenberg-Richter

law. A physical interpretation is that large cracks (which lead to high amplitude AE) occur due to the coalescence of several small cracks (which emit lower amplitude AE). So at any time, we would expect to have more small cracks propagating than large cracks, and this in turn leads to more low amplitude than high amplitude AE. Similar behaviours should be evident in any material where fracture is fractal, or where fracture occurs due to the evolution of cracks with a self-similar distribution of crack lengths (Sammonds et al., 1994). Indeed, in many sets of AE measurement, log (cumulative number of hits), plotted as a function of hit amplitude, forms a straight line. The slope of this straight line is known as the *b-value*. Higher b-values indicate greater ratios of low amplitude hits to high amplitude hits. b-values change as the material (here, natural sea ice) changes. In particular, b-values are expected to decrease during sustained loading, as more and more small cracks join up into larger cracks.

Cumulative magnitude distributions are plotted for all data in the compression experiment (figure 7) and for the indentation experiment (figure 8). In both cases, the data clearly fall on a straight line. Further, in both cases, the slope of these lines is approximately consistent across channels. (Note that in figure 8, data from channel 2 are not shown as the electronics were saturated on this channel). We also see that the slope is not consistent across *experiments* – the b-value calculated for figure 7 (compression) is 1.80 and for figure 8 (indentation) is 1.53. b-values are higher in the compression test than in the indentation test. Similar investigations may allow us to test how confinement (e.g. in the indentation test) affects crack development (Schulson et al., 1991).

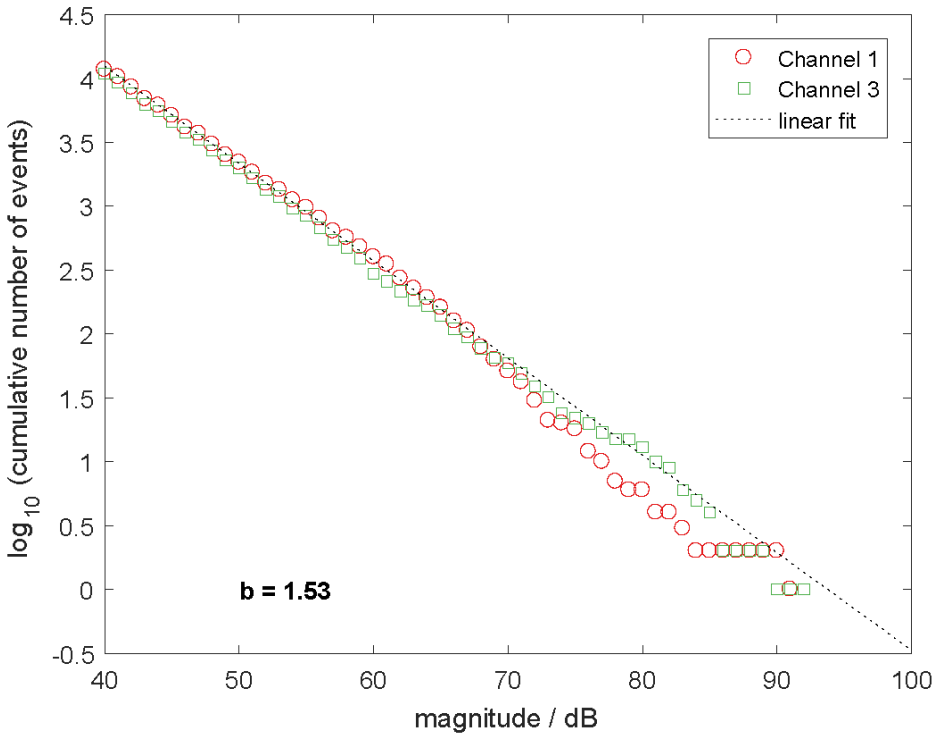

Figure 8: cumulative magnitude distribution for the indentation experiment. Again, the AE follows a Gutenberg-Richter-type behaviour.

b-value variation over time

Within each experiment, we can observe how the b-values change over time. We expect that when the ice is deformed, small cracks will grow and merge, and so the number of large cracks will increase relative to the number of small cracks. In turn, the number of large AE events will increase, relative to the number of small AE events; and so the b-value will decrease over time.

b-values as a function of time are shown in figure 9 (compression experiment) and figure 10 (indentation experiment). In both cases, we group hits into consecutive clusters of ~1000 (occasionally adjusted slightly to avoid clusters which span saturation gaps in the data). So in comparison with figures 7 and 8, where the plots and b-values represent the distribution over the whole experiment, we now calculate b-values averaged over around 1000 data points, encompassing smaller time windows (the relevant time windows are shown as horizontal bars in figures 9 and 10). In figure 9, we see relatively high b-values before loading and at the start of loading (e.g. 0-50s); these then decrease during periods of loading (e.g. 50-150s); and they gradually increase again during periods of relaxation after loading (e.g. 150-550s). In figure 10, where loading is continuous, we see a gradual decrease in b-values over time. We note that this behaviour (as with all AE behaviour) is stochastic, and although overall trends may be apparent, individual data points may not fall in line with these trends.

We conclude that b-value evolution can provide information about the development of microcracking within natural sea ice in situ. In similar experiments on e.g. rocks, concrete and steel, b-values have been used as a predictor of criticality and failure (e.g. Sammonds et al., 1992; Main et al., 1993; Sammonds and Ohnaka, 1998; Colombo et al., 2003, Ramadan et al., 2008)). b-values around 1.5 indicate criticality – the point at which damage in the material begins to localise rather than being uniformly distributed – while b-values tend to <=1 at failure (Sammonds et al., 1992; Carpinteri et al., 2009). Li and Du, 2016, measure b-values during tests on fresh ice in the laboratory and find decreasing b-values during loading which fall close to 1 at the point of failure. The results reported here for natural sea ice are broadly in line with these studies on other materials.

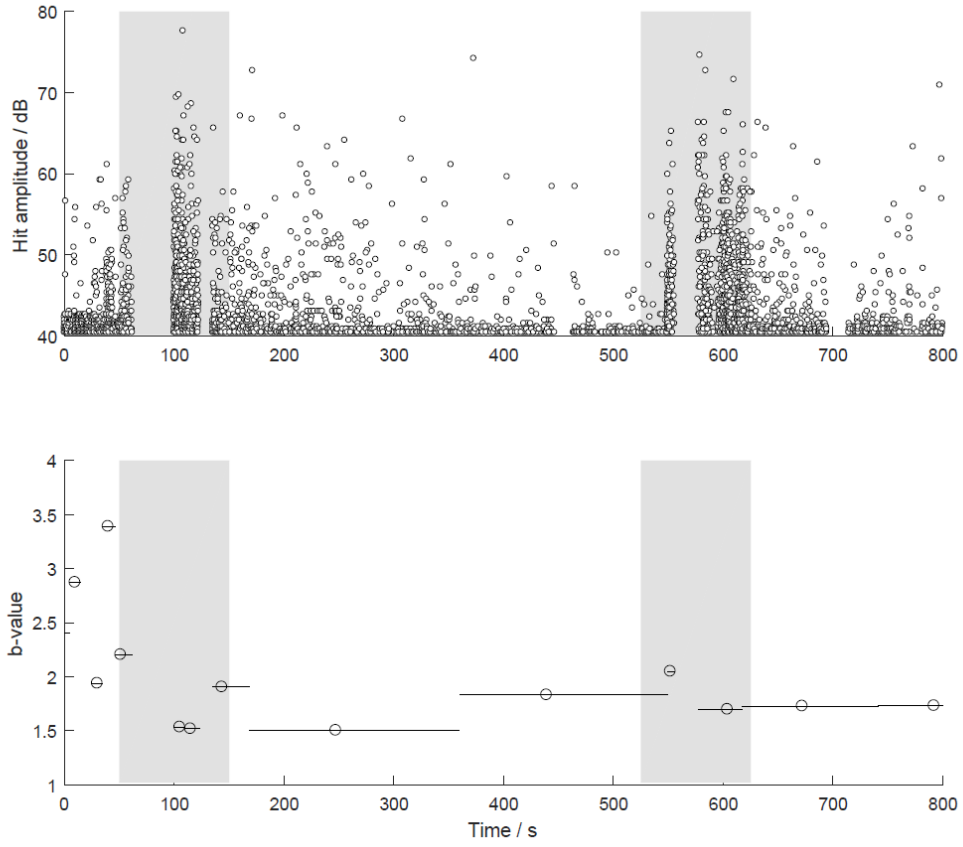

Figure 9: b-value variation during the compression experiment, on channel 1 as a function of time (lower plot). The upper plot repeats the hit intensity data from figure 2, channel 1. Grey boxes match those on figure 2, and show the regions which are shown in more detail in figures 3 and 4. We select channel 1 as the only channel with > 5,000 data points. Each marker in the lower plot shows the b-value calculated for groups of ~1000 data points (sometimes adjusted to fit around breaks in the data). The horizontal lines show the temporal range of these groups of data points. b-values are relatively high at the start of the experiment, and on resumption of loading (around 550s).

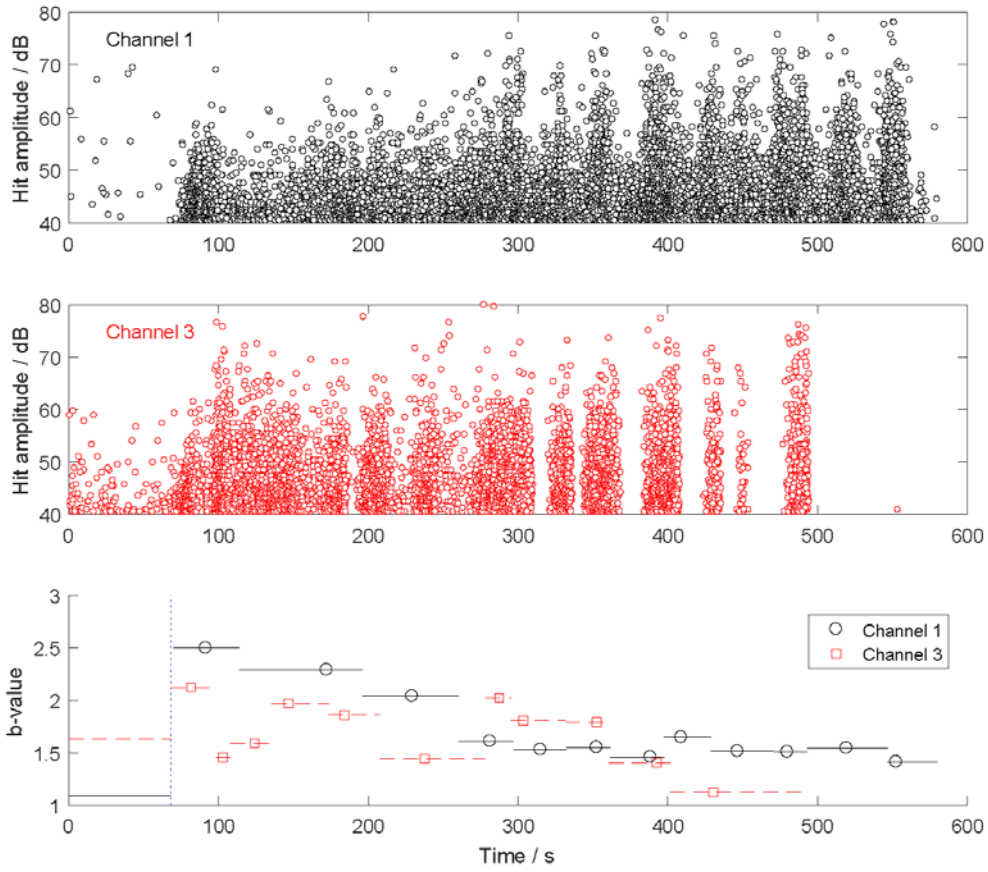

Figure 10: b-value variation against time for the indentation experiment, on channel 1 (black circular markers) and channel 3 (red square markers). b-values are high on initial loading and decrease during the experiment.

Discussion

In this paper we present evidence from two field experiments on sea ice in its natural environment. In both experiments, the ice is loaded in compression: in the first experiment, a broad and flat plate is used to compress the ice, so that compressive stresses are distributed broadly; and in the second, a narrow semicircular indenter is used so that high local stresses occur and the ice is crushed. During each experiment, acoustic emissions are recorded, so that we have information on tens of thousands of individual acoustic events.

In both experiments, AE amplitudes and AE hit counts are associated with load. When the load is applied, we see increased acoustic emissions, and subsequent increases or decreases in load are tracked by equivalent increases or decreases in AE. During cyclic oscillations in the load during the indentation experiment, we observe cyclic oscillations in the AE outputs. One practical outcome of this is that when loading is sporadic, AE can be used to determine when loading periods occur, and when peaks of loading occur within these periods. We also observe that acoustic emissions remain elevated after loading is removed, and decay to their original levels over periods on the order of

100s in our experiments. The elevated AE after loading is removed may represent stress redistributions within the ice (the kind of slow return to an initial unstressed state that might be described by a viscoelastic model), but might also be caused by movements of broken ice fragments. Future lab experiments, which can be controlled more closely than field experiments, could test for AE during relaxation after failure.

Within each experiment, cumulative magnitude plots are presented. These plots show that the magnitudes of AE received obey Gutenberg-Richter scaling laws, and cumulative magnitudes fall in a straight line on a plot of the logarithm of the number of events as a function of the event magnitude in dB. This supports the hypothesis that crack distribution within the ice is self-similar, i.e. it has a fractal distribution. The slope of these cumulative magnitude plots, known as the b-value, is useful as a single number quantifying the ratio of smaller cracks to larger cracks. As the ice evolves towards failure under loading, the b-value is seen to decrease, tending towards a value close to 1, in both experiments. In the compression experiment, the b-value increases during a period of unloading/relaxation. This suggests that AE monitoring and real-time calculation of b-values may be useful as a tool to predict failure in sea ice.

The conclusions drawn above are predicated on three assumptions. First, we have to assume that the sounds being recorded are the sounds of cracking in the ice (rather than, for example, mechanical noise from the actuator pumps). Second, we have to assume that if a received signal is relatively loud, on average that means that it represents a relatively large cracking event. An alternative hypothesis is that most cracks have the same amplitude, and the ones we hear as loud are simply closer to the transducer. Third, we have to assume that the time at which we hear the crack is representative of the time at which it occurred, allowing for some travel time between the crack and the transducer (i.e. we assume that the events are not reordered or delayed by the hardware or software.) We believe that each of these assumptions seems reasonable, given the evidence presented in this paper and elsewhere in the literature on acoustic emissions.

Acoustic emissions may be developed in the future to reveal more information about ice, relevant to applied ice mechanics. At the moment we can only usefully compare amplitudes within experiments. To compare amplitudes across experiments, we would need to first investigate attenuation within the ice, and attenuation in the coupling between the ice and transducer. With our current understanding, we can't tell whether an experiment with relatively low amplitudes has less cracking, or whether the sounds are more attenuated before reaching the transducer. Similarly, it would be useful to have a clear method of comparing between different hardware setups: this would involve comparing the frequency responses of different transducers. If this were achieved, then it might be possible to estimate energies of cracking and move towards a non-invasive method of load measurement in ice. Second, it may be possible to distinguish between different crack modes by considering the properties of the received transient (Li and Du, 2016). Third, it would be useful to correlate individual events across multiple transducers. If an event can be recorded on two transducers, we can get a linear estimate of its location; on three transducers, a planar estimate; and if the sound is recorded on four or more transducers we may be able to estimate its origin in 3D space (using the techniques of multilateration). Mackenzie et al., 2000, are able to locate individual events during fracture of cantilever beams, using a four transducer array. In turn, if we can record

the time and location of individual cracks, we can develop our understanding of how crack networks develop to failure in sea ice under load (multilateration to locate failure in rocks is demonstrated in e.g. Heap et al., 2009). Location of crack sources would also allow us to make inferences about attenuation, and hence to infer the amplitude at the source of each crack, which might in turn allow us to provide estimates of the total energy dissipated in cracking within a given region of the ice. Further, if we could locate cracks then we could begin to observe differences in properties through the ice sheet. The emissions detected in this paper are more likely to come from the top surface of the ice (since that is where the transducers are placed) than the columnar structure underneath. Future work could consider how emissions might vary with source depth in the ice.

We also note that acoustic emissions analysis, of the kind reported in this paper, is becoming more feasible in field conditions. In this paper we measure acoustic emissions from in-situ sea ice in the frequency range from 100-180kHz, and are able to record associated waveforms. To achieve this, we need to record at sample rates of around 360kHz or higher. Until quite recently, these sample rates have required high-specification bespoke electronics. Often these electronic systems have been configured for the laboratory and have been unsuitable for the field, due to weight, bulk, fragility, and the need for a continuous power supply. In the last ten years, advances in consumer electronics have led to advances in lab and field kit, and it's now possible to record gigabytes of AE data using equipment which will fit in a small rucksack. One aim of this paper is to demonstrate some of the measurement and analysis which could be made using current equipment. We acknowledge the irony that our measurements were made on equipment which was heavy, bulky, fragile, and needed a continuous power supply. In spite of this, the amount of AE data recorded in these experiments would not have been practical in the 20th century, but is now achievable in remote field locations.

Conclusions

- We present a new large data set of acoustic emissions from compressive tests on natural sea ice in the field.
- We show that AE hit rates and maximum amplitudes rise and fall as the compressive load on the ice rises and falls.
- We show that AE from these experiments obey Gutenberg-Richter scaling laws, and that b-values tend to decrease towards one as ice is damaged, and increase again when loading is removed.
- We propose that acoustic emissions measurements can be used to make inferences about processes of damage and healing in natural sea ice in situ.

Acknowledgments

The authors wish to acknowledge the support of the Research Council of Norway through the SFI SAMCoT. The authors thank Alexander Sakharov, Evgeny Karulin, Marina Karulina and Petr Chistyakov for organising the ice deformation experiments.

Competing interests
The authors have no competing interests to declare.

References
Carpinteri, Alberto, Giuseppe Lacidogna, and Simone Puzzi. "From criticality to final collapse: Evolution of the “b-value” from 1.5 to 1.0." Chaos, Solitons & Fractals 41, no. 2 (2009): 843-853.

Chistyakov, Karulin, Marchenko, Sakharov, Lishman, 2016. Tensile strength of saline and freshwater ice in field tests. In proc. 23rd IAHR International Symposium on Ice, Ann Arbor, Michigan USA, 31st-3rd June 2016.

Cole, D. M., & Dempsey, J. P. (2004). In situ sea ice experiments in McMurdo Sound: cyclic loading, fracture, and acoustic emissions. Journal of cold regions engineering, 18(4), 155-174.

Cole and Dempsey, 2006. Laboratory observations of acoustic emission from Antarctic first-year sea ice cores under cyclic loading. In proc. 18th Int. Conf. on Port and Ocean Eng. Under Arctic Conditions, Vol 3, 1083-1092.

Colombo, Ing S., I. G. Main, and M. C. Forde. "Assessing damage of reinforced concrete beam using “b-value” analysis of acoustic emission signals." Journal of materials in civil engineering 15, no. 3 (2003): 280-286.

Gagnon, R. E. "An explanation for the Molikpaq May 12, 1986 event." Cold Regions Science and Technology 82 (2012): 75-93.

Gold, Lorne W. "The cracking activity in ice during creep." Canadian Journal of Physics 38, no. 9 (1960): 1137-1148.

Heap, M. J., P. Baud, P. G. Meredith, A. F. Bell, and I. G. Main. "Time-dependent brittle creep in Darley Dale sandstone." Journal of Geophysical Research: Solid Earth 114, no. B7 (2009).

Kaiser, J, 1953. Untersuchungen uber das auftreten Geraushen beim Zugversuch, Ph.D. Thesis, Technische Hochschule, Munich (1950); se e also Arkiv Fur das Eisenhuttenwesen 24, 43.

Karulina, M., A. Marchenko, E. Karulin, D. Sodhi, A. Sakharov, and P. Chistyakov. "Full-scale flexural strength of sea ice and freshwater ice in Spitsbergen Fjords and North-West Barents Sea." Applied Ocean Research 90 (2019): 101853.

Kishinoue, F, 1990. An experiment on the progression of fracture (a preliminary report). Jisin 6:24-31 (1934), translated and published by Ono, K, Journal of AE 9(3): 177-180.

Langhorne, P.J., Robinson, W.H., and Squire, V.A., 1990. “Acoustic emission generated by moving loads on sea ice: preliminary results”. Cold Regions Science and Technology, 18/3, pages 337-342.

Langhorne, P. J., M. F. Tan, and B. D. Russell. "Preliminary measurements of acoustic emission in young artificial sea ice." In The Third International Offshore and Polar Engineering Conference. International Society of Offshore and Polar Engineers, 1993.

Langhorne, P. J., and T. G. Haskell. "Acoustic emission during fatigue experiments on first year sea ice." Cold regions science and technology 24, no. 3 (1996): 237-250.

Langley, A. J. "Acoustic emission from the Arctic ice sheet." The Journal of the Acoustical Society of America 85, no. 2 (1989): 692-701.

Li, Dongsheng, and Fangzhu Du. "Monitoring and evaluating the failure behavior of ice structure using the acoustic emission technique." Cold Regions Science and Technology 129 (2016): 51-59.

Liptai, R. G., D. O. Harris, R. B. Engle, and C_ A. Tatro, 1970. Acoustic emission techniques in materials research. No. UCRL--72582. California Univ.

Mackenzie, C., Langhorne, P.J., and Haskell, T.G., 2000. Acoustic emission location and cracking in sea ice. In proc. 15th IAHR International Symposium on Ice, Gdansk, Poland, August 28-September 1 2000, volume II, pps. 71-79.

Main, Ian G., Peter R. Sammonds, and Philip G. Meredith. "Application of a modified Griffith criterion to the evolution of fractal damage during compressional rock failure." Geophysical Journal International 115, no. 2 (1993): 367-380.

Mansurov, V. A. "Acoustic emission from failing rock behaviour." Rock Mechanics and Rock Engineering 27, no. 3 (1994): 173-182.

Marchenko, A., Karulin, E., Karulina, K., Sakharov, A., Chistyakov, P., Sodhi, D., and Sliusarenko, A., 2018. “Scale effects in compressive strength of sea ice.” In proc. 24th IAHR International Symposium on Ice, Vladivostok, Russia, June 4th-8th 2018.

Ramadan, Salah, Laurent Gaillet, C. Tessier, and Hassane Idrissi. "Detection of stress corrosion cracking of high-strength steel used in prestressed concrete structures by acoustic emission technique." Applied surface science 254, no. 8 (2008): 2255-2261.

Rist, M.A. and Murrell, S.A.F., 1990. Examination of semi-brittle uniaxial and triaxial deformation behaviour of polycrystalline ice using acoustic emission measuring technique. In: Proc. 2nd International Conference on Ice Technology, Cambridge, pp. 91-102.

Sammonds, Peter R., P. G. Meredith, and I. G. Main. "Role of pore fluids in the generation of seismic precursors to shear fracture." Nature 359, no. 6392 (1992): 228.

Sammonds, Peter R., P. G. Meredith, S. A. F. Murrell, and I. G. Main. "Modelling the damage evolution in rock containing pore fluid by acoustic emission." In Rock Mechanics in Petroleum Engineering. Society of Petroleum Engineers, 1994.

Sammonds, Peter R., and Mitiyasu Ohnaka. "Evolution of microseismicity during frictional sliding." Geophysical Research Letters 25, no. 5 (1998): 699-702.

Schulson, E. M., D. E. Jones, and Go A. Kuehn. "The effect of confinement on the brittle compressive fracture of ice." Annals of Glaciology 15 (1991): 216-221.

Sinha, N.K., 1982. Acoustic emission and microcracking in ice. Proc. SESA/Japan Soc. for Mech. Eng., Hawaii, Vol. 2, pp. 767-772.

Sinha, 1985, Acoustic emission study on multi-year sea ice in an Arctic field laboratory. J. Acoust. Emission, 4 (2/3) (1985), pp. S290-S293

Sinha, N.K., Zhan, C., and Evgin, E., 1992. Creep of sea ice. Proc. of 11th Intl. Conf. on Offshore Mechanics and Arctic Engineering, Calgary, June 1992, Vol. 4 (1992), pp. 261-266

Sinha, N.K., 1996. Characteristics of acoustic emissions from different types of polycrystalline ice. In: Proc. International Symposium on Snow and Related Manifestations, Manali

St Lawrence, William F., and David M. Cole. Acoustic emissions from polycrystalline ice. No. CRREL-82-21. Cold Regions Research and Engineering Lab. Hanover NH, 1982.

Weiss, Jerome, and Jean-Robert Grasso. "Acoustic emission in single crystals of ice." The Journal of Physical Chemistry B 101, no. 32 (1997): 6113-6117.

Xie, Yunbo, and David M. Farmer. "Acoustical radiation from thermally stressed sea ice." The Journal of the Acoustical Society of America 89, no. 5 (1991): 2215-2231.

Appendix - AE from a single transducer monitoring a tensile test

To demonstrate some basic properties of AE measurement in ice, we consider the recorded output from a single transducer during a simple tensile test. A vertical sea ice core is flattened on both ends and frozen into end caps using fresh water. These end caps are then pulled apart on a bespoke testing rig until the ice fails in tension. The cores have diameter 72.5mm, and the caps have inner diameter 80mm and wall height of 50mm. Steel rods are used to keep the caps coaxial while the core is frozen in over several hours. The load is applied by an Enerpac 15T hydraulic cylinder. The acoustic transducer is frozen onto the outside of the top cap using fresh water. Further experimental details can be found in Chystyakov et al., 2016. The experiment is shown in figure A1a, and the recorded tensile force and acoustic emissions are shown in figure A1b.

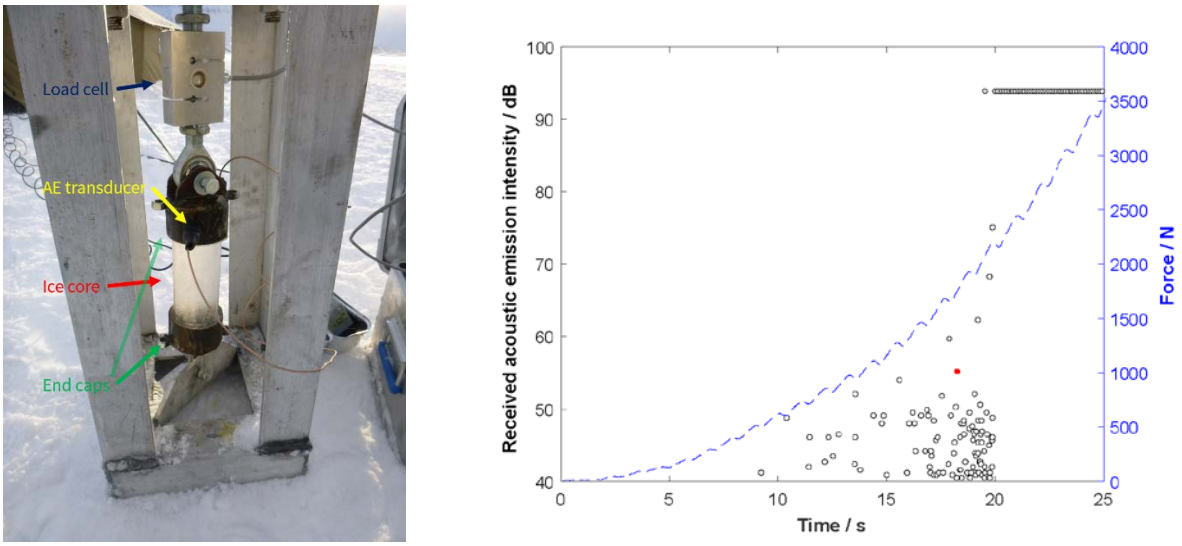

(a) (b)

Figure A1: acoustic emissions from a tensile test in the field. The left hand figure shows the test setup. The right hand figure shows the measured force (blue dashed line, right hand y-axis) and the recorded acoustic emission hits (circular markers, left hand y-axis).

It is useful to describe some features of the results. The load applied to the ice increases throughout the experiment, and failure occurs after around 30s. The acoustic emissions results are shown in figure A1b as *hits*, where each hit corresponds to a specific acoustic event. It can be helpful to think of each hit (i.e. each circle on figure A1b) as representing a single 'ping', perhaps due to a single crack propagation event in the ice. The hits are represented here in terms of their recorded amplitude and time. Markers which are higher up the graph represent hits which are louder at the receiver. This in turn might indicate that they were louder at their source, that they occurred closer to the receiver, or that they were less attenuated between source and receiver.

The force and AE measurements were recorded on separate systems with no synchronisation signal. The time axes for these two signals, therefore, cannot be accurately aligned. Direct observation of the experiments confirms that the burst of AE visible in figure A1b occurred during the increase in load. A second significant problem with these experiments is clear after around 20s on the graph: our system saturates and records only a continuous stream of maximum-intensity hits (around

94dB, here). We are unable to ascribe any meaning to the amplitudes measured after this saturation occurs. After the ice fails at around 30s, saturation in the AE continues as the two loose ends of the ice move freely and AE is generated from friction around the moving cap fittings.

In spite of these limitations, we can draw some important conclusions from this experiment. First, we note that the acoustic emissions are stochastic in nature. Although the force increases near-monotonically, the acoustic emissions go up and down in intensity over time. Within this stochastic behaviour, two patterns emerge. First, as the force increases, the occurrence of acoustic hits tends to increase (i.e. we see more hits towards the right of figure A1b). Second, as the force increases, the maximum intensity of hits tends to increase (i.e. we see higher amplitudes towards the right of figure A1b). These two trends can be seen in figure A2.

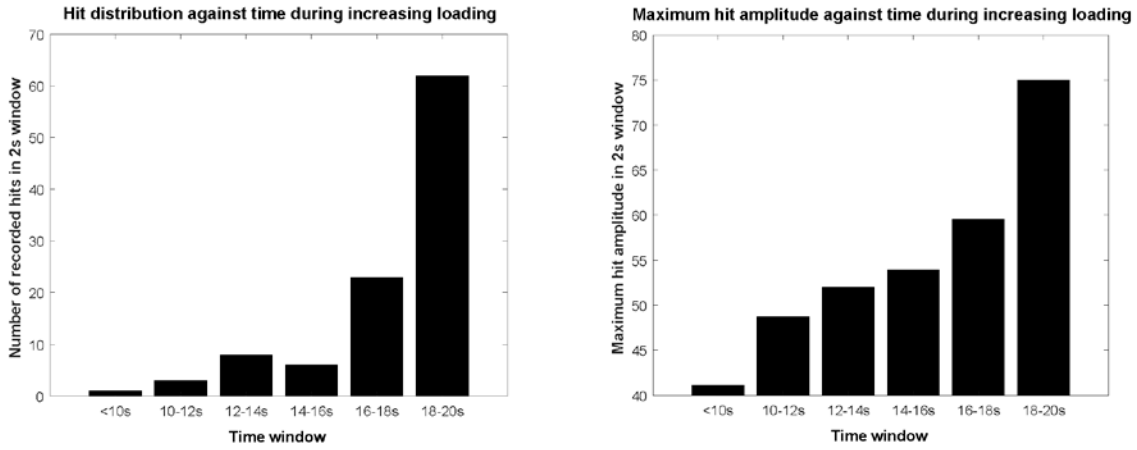

(a) (b)

Figure A2: number of recorded hits per 2s time window (LHS, a) and maximum hit amplitude in the same 2s window (RHS, b), during the period of increasing load in the tensile test shown in figure A1.

Finally, these experiments also allow us to investigate the waveforms associated with each individual hit (the 'transients'). The red marker in figure A1b, for example, which corresponds to the 253rd hit measured in the experiment, has a maximum amplitude of 55.1dB and a peak frequency component of 110kHz. Its waveform and the FFT of its waveform are shown in figure A3. The FFT is derived from unfiltered data sampled at 5MSs^{-1}.

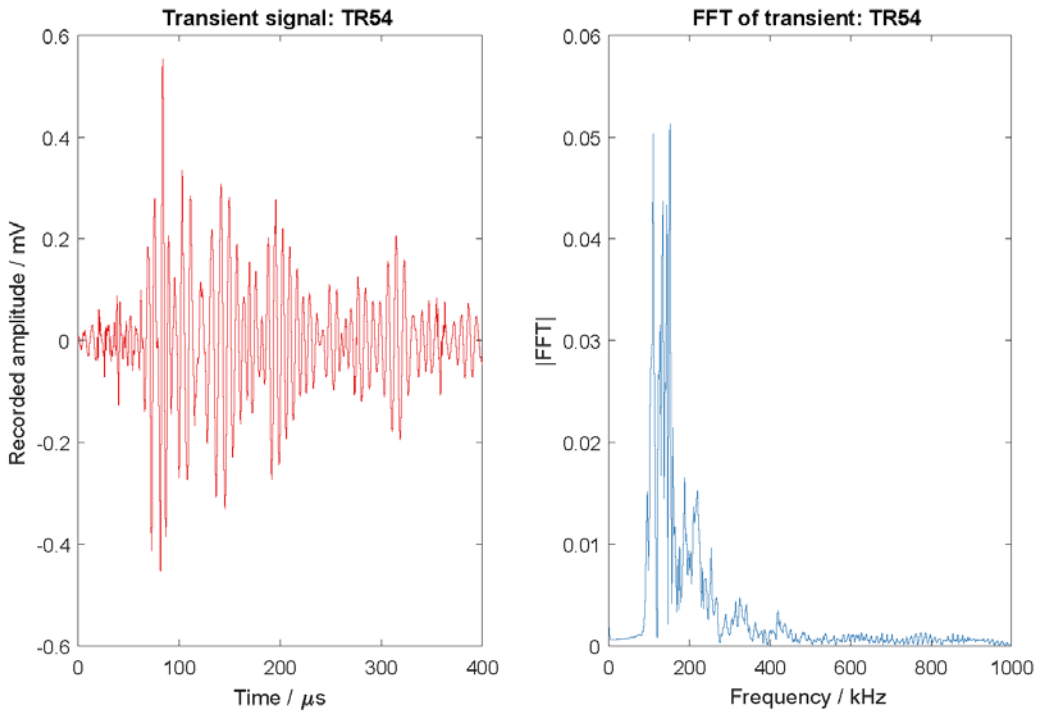

Figure A3: the left hand figure shows the waveform – amplitude against time – for the hit represented by the red marker in figure A2b. The right hand figure shows the magnitude of the FFT of this waveform, which has a peak around 110kHz.